North and northeast Greenland ice discharge from satellite radar interferometry

E.J. Rignot[1], S.P. Gogineni, W.B. Krabill, and S. Ekholm

Ice discharge from north and northeast Greenland calculated using satellite radar interferometry data of fourteen outlet glaciers is 3.5 times that estimated from iceberg production. The satellite estimates, obtained at the grounding line of the outlet glaciers, differ from those obtained at the glacier front because basal melting is extensive at the underside of the floating glacier sections. The results suggest that the north and northeast parts of the Greenland ice sheet are thinning and contributing positively to sea-level rise.

Science

[1]E.J. Rignot, Jet Propulsion Laboratory, California Institute of Technology, Pasadena, CA 91109-8099, USA; S.P. Gogineni, Radar Systems and Remote Sensing Laboratory, The University of Kansas, 2291 Irving Hill Road, Lawrence, KS 66045-2969, USA; W.B. Krabill, NASA Goddard Space Flight Center, Wallops Flight Facility, laboratory for Hydrospheric Processes, Wallops Island, VA 233337, USA; S. Ekholm, Kort & Matrikelstyrelsen, Geodetic Division, Rentemestervej 8, 1)1(-2400 Copenhagen NV, Denmark

The traditional view on the mass balance of the Greenland ice sheet is that accumulation of mass (mostly snow) in the interior regions is released to the ocean through surface ablation (or melting) and calving of icebergs (*1*). Of all three components of the mass balance, snow accumulation is the best known from snow pits and ice cores measurements across the ice sheet (*2*). Observations of surface melt rates are comparatively limited and restricted to the western marginal zone (3). Iceberg calving is the least-well known (*4*). Iceberg production has been estimated in the west (5), north and northeast (6) by means of repeated aerial photography. The velocity of the calving front is measured by tracking distinctive patterns of crevasses over time. Ice thickness is deduced from tile height of the calving front. Immediately inland of the calving front, ice thickness is not well known (*7*), surface features are more subdued, and locating the grounding line, which is where a glacier detaches from its bed to become afloat in the ocean, is difficult (*8*).

Satellite radar interferometry permits a systematic, detailed, and precise mapping of the grounding line of outlet glaciers (9, 10). The grounding line is a natural boundary for calculating ice discharge because the entire ice volume that crosses it eventually melts into the ocean. Here, we mapped tile grounding line of north and northeast Greenland glaciers (*11*) (Fig. 1 and 2) using radar data from the Earth Remote Sensing Satellites (ERS-1 and 2), and estimated their ice discharge at the grounding line. This part of Greenland includes large sections of floating glacier ice, which are preserved because of the low glacier slopes, combined with the constraining effect of permanent sea-ice in the fjords (*12*).

We used a high-quality digital elevation model (DEM) of north Greenland (*13*) to estimate the thickness of the floating glacier sections in this region assuming that the glacier ice is in hydrostatic equilibrium (*14*). To assess the accuracy of the method, we compared the elevation data to ice thick ness data obtained by an ice

sounding radar (ISR) (*15*), and laser altimetry data (AOL) (*16*) collected along single longitudinal profiles crossing the grounding line of the three largest glaciers (Fig. 2 ancl 3). The comparison shows that hydrostatic equilibrium is first reached about 1 to 2 km downstream from the interferometrically-derived grounding line or hinge line (*11*). Near that location, the DEM-derived thickness is within 10% of the AOL-derived thickness and the ISR data.

Ice discharge was calculated along profiles located 1 km downstream from the hinge line and parallel to it as the integral of the product of the I)I~M-derived ice thickness with the velocity component perpendicular to the grounding line. Over the floating section of a glacier, the vertical gradient in velocity is negligible (*17*), so the ERS-derived velocities represent vertically integrated velocities. The actual ice velocity vectors were obtained by combining the line of sight component of the velocity procured by radar interferometry with flow direction information provided by the prominent glacier flow lines in the radar amplitude images (Fig. 2). The precision of the measured perpendicular component of the ice velocity is 4% (*18*).

Combined together, the analysis implies that the 14 glaciers discharge 49.2 km^3/yr of ice into the ocean (10% uncertainty) (l'able 1). This ice volume is 3.5 times that discharged at the glacier front (6). The largest difference is recorded on Petermann Gletscher, where the grounding line flux is 22 times the glacier front flux.

If the floating glacier sections are in steady-state conditions, the ice flux decrease implies that they are melting (*19*). If they are not in steady-state, they should be thickening instead, because not enough ice passing the grounding line reaches the glacier front. AOL data collected in 1995 and 1996011 Petermann Gletscher, however, indicate that the glacier tongue did not thicken at detectable levels (1 m) over 1 year. We therefore assume that the ice tongue is in steady-state and the ice flux decrease is due to melting. On Petermann Gletscher, the inferred steady-state melt rate is

12 m/yr, and peak values exceed 20 m/yr near the grounding line (*10*).

The few observations in north and northeast Greenland suggest that surface melt rates are less than 3 m/yr (*20*). The only possible explanation for the ice flux decrease is then that the ice tongues loose mass through extensive melting at the base of the glaciers. If we assume a surface melt rate of 2 m/yr for the floating tongues (6), basal melting must average 10 m/yr on Petermann Gletscher, S m/yr on Nioghalvfjerdsbræ, and 6 m/yr on Zachariae Isstrøm to explain the results in Table 1. These values are high compared to the 1 to 2 m/yr average basal melt rate of Antarctic ice shelves (*21*), but comparable to the localised high basal melt rates (7 to 10 m/yr) measured on several Antarctic tidal outlet glaciers (*22*).

'I'he outlet glaciers of north and northeast Greenland will maintain a state of balance if the mass discharged at the grounding' line is compensated by an equal amount of mass accumulating in the interior regions nourishing them with glacier ice. over our study area, the predicted balance grounding line discharge is 21 km^3/yr (*23*), which is less than half the 49-km^3/yr discharge that we measured at the grounding line. If these estimates are correct, this means that north and northeast Greenland glaciers discharge an excess 28 km^3/yr glacier ice into the ocean, which is equivalent to a 26-Gt/yr mass loss (with an ice density of 0.91 7) or a 0.07-mm sea-level rise. The northern sector of the Greenland Ice Sheet is therefore thinning and gives a positive contribution to sea-level rise.

Our results cannot be extrapolated easily to the entire ice sheet because small floating glacier sections exist elsewhere, for example along tile western coast (5, *12*). These floating sections may still generate large amounts of basal melt water because basal melting is often most pronounced near the grounding line, where tidal pumping is most efficient and where the glacier draft reaches the deepest waters (*21* – 22).

REFERENCES AND NOTES

1 N. Reeh, in *Quaternary geology of Canada and Greenland*, R. J. Fulton, Ed. (Geological Survey of Canada, Geology of Canada, 19S9) Chapt. 14, pp. 793-822; C. S. Benson, *U.S. Army Cold Reg. Res. Eng. Lab. Rep. ?'0* (Hanover, NH) (1962); A. Weidick, *Gletscher-hydrologiske Meddelelser 85, (1985);* H. Bader, *U.S. Army Cold Reg. Res. Eng. Lab. Rep. I-B2* (Hanover, NH) (1961); F. Loewe, *Beiträge zur Geophysik* 46, 317 (1936).

2 A. Ohmura ant] N. Reeh, *J. Glaciol. 37,* 140 (1991).

3 R. Braithwaite, *Grønlands Geologiske Undersøgelse* 98, (19S0).

4 N. Reeh, *Report of a Work-shop Held in Seattle, Washington, 13-15 September 1984, Washington D. C.* (National Academy Press, 19S5), pp. 1,55-171.

5 M. Carbonnell and A. Bauer, *Meddelelser* om *Grønland 173 (196 S); R. C.* Kollmeyer, in *World Glacier Inventory, Proceedings of a Workshop at Riederalp, Switzerland, 17-22 September 1978* (International Association of Hydrological Sciences) 126, pp. 57-65 (19S0).

6 A. Higgins, *Grønlands Geologiske Undersøgelse 140 (1988);* A. Higgins, *Polar Forschung* 60, 1 (1990).

7 P. Gudmandsen, in *Remote Sensing of the terrestrial environment 28*, R. F. Peel, L. F. Curtis, E. C. Barret, Eds. (Colston Papers, Bristol, 1977), pp. 19s-211.

S 'I'he grounding line may be located from an examination of small fractures at the surface of a glacier caused by the tidal displacements [S. N. Stephenson, *Ann. Glaciol.* 5, 165 (19 S4)], or using a radio echo sounder [R. W. Jacobel,

A. E. Robinson, R. A. Bindschadler, ibid. *20,* 39 *(1991)].* The limit of tidal flexing is precisely fount{ using Globs] Positioning System (GPS) surveys and tiltmeters [1). G. Vaughan, ibid. *20,* 372 *(1994); A. M.* Smith. *J. Glaciol. 37, 51* (1991 *)].* The above techniques, 11 owever, are limited in spatial sampling. Visible imagery [C. Swithinbank, K. Brunk, J. Sievers, *Ann. Glaciol.* 11, *150 (1988)]* and radar altimetry [R. 11. Thomas, '1'. V. Martin, H. J. Zwally, ibid. 4, 2S3, (1983)] provide a large scale, uniform sampling view of the grounding zone, but their precision is much less than that of GPS techniques.

9 R. M. Goldstein, H. Engelhardt, B. Kamb, R. M. Frolich, *Science* 262, 1525 (1993).

10 E. Rignot, *J. Glaciol. 42,* 476 *(1996).*

11 To locate the grounding line with ERS radar interferometry, we used two interferograms formed by combining ERS image data acquired 1 day apart. A DEM was registered to each interferogram from a knowledge of the radar imaging geometry and the satellite precision orbits. The phase variations associated with surface topography and the interferometric baseline were then automatically removed from the interferograms, leaving only phase variations caused by the glacier deformation over 1 day. This deformation is the combination of a long-term motion under the driving stress procured by gravity, and a short-term vertical motion induced by tidal forcing from the ocean. If the glacier velocity (or gravity term) is contiguous and steady throughout the period of observation, the differencing of two such interferograms produces a third interferogram which only contains the tidal signal. It is then possible to locate the limit of tidal flexing, or glacier hinge line, within less than 100 m, across the entire glacier width (*10*).

12 1,. Koch, *Meddelelser om Grønland 65* (1 928).

13 S. Ekholm, *J. Geophys. Res.* 101, 21,961 (1996).

14 An accurate measurement of the ice thickness from the glacier surface elevation requires a knowledge of the density profile with depth. We assumed that the mean glacier ice density, ρ_i, is 917 kg/m^3 for the relatively warm ice of the coastal regions [P. V. Hobbs, *Ice Physics* (Oxford Univ. Press, London, 1974)], and the sea water density, ρ_w, is 1030 kg/m^3 [A. Foldvik, T. Gammelsrød, T. Tørresen, *Polar Res.* 3, 209 (19 S5)]. Ice thickness is obtained by multiplying the surface elevation by $\rho_w/(\rho_w-\rho_i)$ or 9.115.

15 '1'. S. Chuah, S. P. Gogineni, C. Allen, B. Wohletz, *Radar* Systems *and* Remote Sensing *Laboratory Tech. Rep. 10470*, (University of Kansas, Lawrence, Kansas, 1996).

16 W. B. Krabill, R. H. Thomas, C. F. Martin, R. N. Swift, E. B. Frederick, *Int. J. Rem. Sens.* 16, 1211 *(1995).*

17 '1'. J. O. Sanderson and C. S. M. Doake, *J. Glaciol.* 22, 2S5 (1979).

1S Ice flow direction is known within 5 degrees. The line of sight interferometric velocity is known within 2 mm/d or 1 in/yr. The ERS data had a line of sight vector within 30 degrees of the main flow direction.

19 W. S. B. Paterson, *The* physics *of glaciers* (Elsevier Science, Tarrytown, NY, 1994).

20 C. E. Bøggild, N. Reeh, H. Oerter, *Global and Planetary Change* 9, 79 (1994); T. Konzelmann and R. Braithwaite, *J. Glaciol.* 41, 174 (1995); T. Høy, *Meddelelser om Grønland 182* (1970).

21 S. S. Jacobs, H. H. Helmer, C. S. M. Doake, A. Jenkins, R. M. Frolich, *J. Glaciol.* 38, 375 (1992); A. Jenkins and C. S. M. Doake, J. *Geophys. Res.* 96, 791 (1991); D. R. McAyeal, *J. Geophys. Res.* 89, 597 (19S4).

22 S. S. Jacobs, 11.11. Helmer, A. Jenkins, *Geophys. Res. Lett.* 23, 957 (1996); A. M. Smith, *J. Geophys. Res.* 101, 22,749 (1996).

23 'l'he iceberg discharge for an ice sheet in a state of balance was calculated in (*4*). Over our study area, the total is 14 km^3/yr. To translate that number into a balance ice discharge at the grounding line, we need to add to this total the ice volume lost by surface ablation from the floating ice tongues, which we estimated using the ablation rates in (3), the ERS images, and the DEM to be 7 km^3/yr.

24 G. Holdsworth, *J. Glaciol.* 8, 3S5 (1969); G. Holdsworth, *Ann. Geophys.* 33, 133 (1977).

25 A. Weidick, *U.S. Geol. Surv. Prof. Pap. 1386*, (Denver, CO, 1995).

26 We thank G. Duchossois, G. Kohlhammer, and the European Space Agency for providing radar data, R. H. Thomas for useful discussions, and C. Werner for providing a synthetic-aperture radar processor. This work was carried out at the Jet Propulsion laboratory, California Institute of Technology, under a contract with the National Aeronautics and Space Administration.

FIGURE CAPTIONS

Fig. 1. Location of the 14 outlet glaciers of north and northeast Greenland ant] the ERS frames used in this study. Each ERS scene is 100-km^2.

Fig. 2. Tidal displacements of the floating section of (A) Petermann Gletscher, (B) Nioghalvfjerdsbræ, and (C) Zachariae Isstrøm obtained from quadruple-difference ERS radar interferometry. Each fringe, or 360° variation in phase, represents a 28 mm displacement of the glacier tongue toward the radar line of sight (23° away from vertical) due to forcing by the ocean tide. The phase image is modulated by the radar brightness of the scene. The hinge line, or limit of tidal flexing, is shown in clots. The amplitude of the tidal displacements raises quickly from the hinge line (high fringe rate) and subsequently decreases slowly toward the glacier front. This deformation pattern agrees with model predictions from an elastic beam clamped at one end on bedrock (hinge line) and freely floating on the ocean (*24*). The location of the ISR and AOL profiles for each glacier is shown in clashes. North (N) is indicated by an arrow. Solid arrows indicate flow direction parallel to flow lines conspicuous in the radar amplitude images. Residual fringes on rock are caused by imperfections in the DEM in areas of high topographic relief.

Fig. 3. Ice thickness derived from laser altimetry (AOL), ice sounding radar (1 SR), and surface elevation (KMS) neat the grounding line (GL, indicated by an arrow) of (A) Petermann Gletscher; (B) Nioghalvfjerdsbræ; and (C) Zachariae Isstrøm, as a function of the distance along the profile. North (N) is indicated by an arrow. The precision of the KMS elevation, AOL elevation, and ISR thickness is, respectively, 10 to 20 m (*13*), 10 cm (*16*), and 10 m (*15*). Georeferencing of the ERS data is accurate to within SO m. The AOL/ISR profile for Nioghalvfjerdsbræ is not optimal because too close to the ice margin and almost parallel to the grounding line (Fig. 2). The

AOL- and KMS-derived thicknesses calculated upstream (south) of the grounding line are in error because the glacier ice is not in hydrostatic equilibrium.

Table 1. Glacier width (W), average velocity (V), average thickness (T), grounding line ice flux (GF), and calving flux (CF) from (*6*) and (CF*) from (*25*) for the outlet glaciers in Fig. 1. W, V and T for Ostenfeld and Brikkerne Gletscher are for the main glacier branch only. Uncertainties in ice thickness greater than 10% are denoted with †. The last line indicates total ice discharge.

Glacier	W km	V m/yr	T m	GF km^3/yr	CF km^3/yr
Petermann Gl.	20.5	1139	614	13.20	0.59
Steensby Gl.	3.4	329	547	0.63	0.32
Ryder Gl.	7.9	506	595	2.55	0.70
Ostenfeld Gl.	7.6	667	541	2.71	0.54
Harder Gl.	4.5	187	340	0.34	0.03
Brikkerne Gl.	3.5	364	160	0.44	0.37
Jungersen Gl.	1.5	395	340†	0.20	0.10
Naravana Fj. Gl.	1.8	59	200†	0.02	0.01
Henson Gl.	2.2	286	123†	0.08	0.04
Marie Sophie Gl.	3.3	40	136	0.02	0.13
Academy Gl.	7.4	290	120	0.26	0.14
Hagen Brae Gl.	7.9	111	731	0.64	0.36
Nioghalvfj. Gl.	21.5	1022	771	15.74	2.80*
Zachariae Is.	19.8	855	647	12.40	7.40*
				49.2	13.5

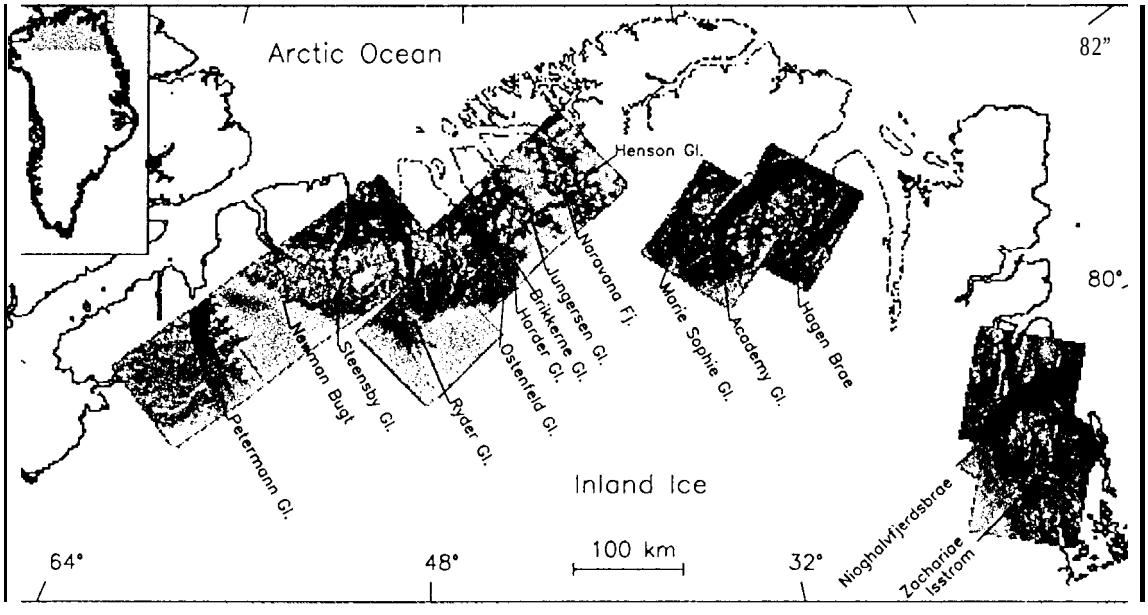

Figure 1, Rignot et al. 970255

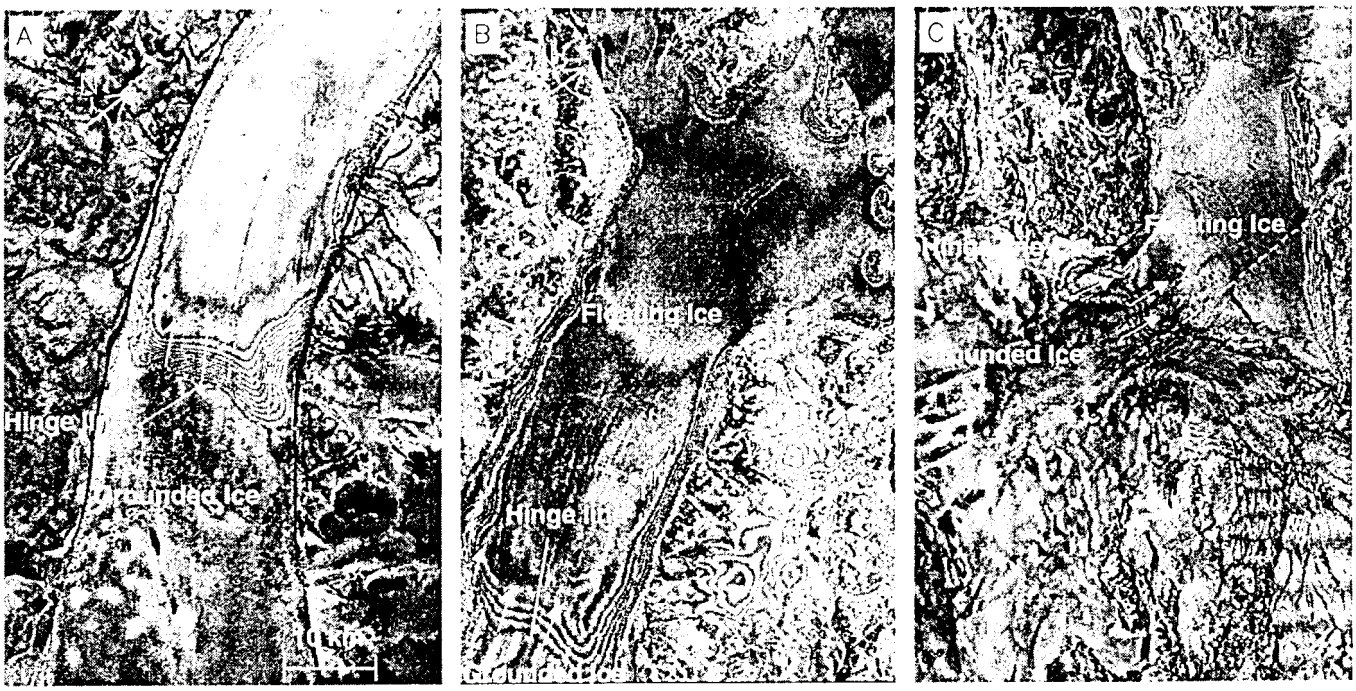

Figure 2, Rignot et al. 9'/0255

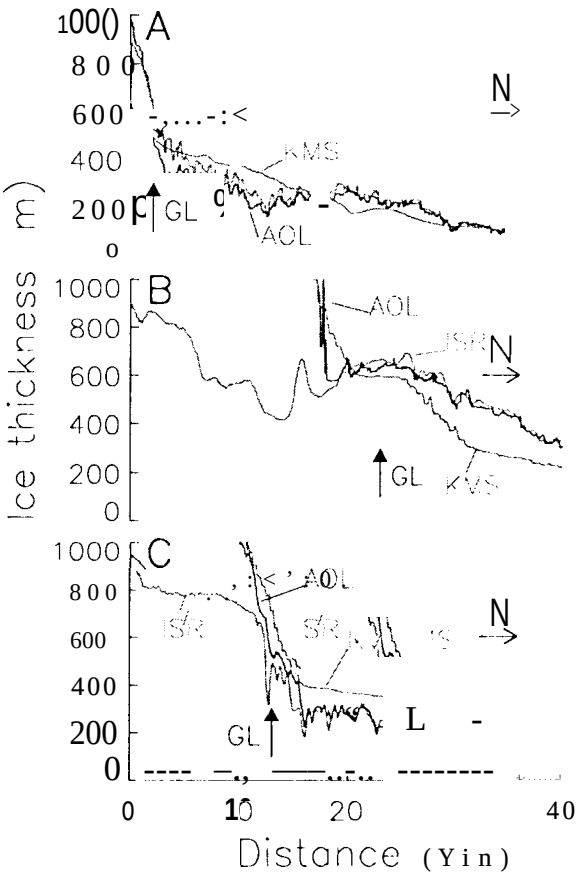

Figure 3, Rignot et al. 970255